Journal of Alloys and Compounds, *195* (1993) 129–132
JALCOM 7431

Microstructure investigations of the epitaxial growth of ultrathin $Bi_2Sr_2CaCu_2O_x$ superconducting films on (001) $SrTiO_3$ substrates

T.Amrein[a,b], B. Kabius[b], J. Burger[c], G. Saemann-Ischenko[c], L. Schultz[a] and K. Urban[b]

[a]) SIEMENS AG, Research Laboratories, P.O. Box 3220, 8520 Erlangen, Germany

[b]) Institut für Festkörperforschung, Forschungszentrum Jülich GmbH, Postfach 1913, 5170 Jülich, Germany

[c]) Physikalisches Institut, Universität Erlangen-Nürnberg, 8520 Erlangen, Germany

Abstract

The microstructure of epitaxial, c-axis oriented $Bi_2Sr_2CaCu_2O_x$ superconducting thin films with a mean thickness of 3 to 100 nm on (001) $SrTiO_3$ substrates was studied by plan-view and cross-section transmission electron microscopy (TEM) and atomic force microscopy (AFM). An inductively measured transition temperature could be observed down to 12.5-nm thick films. In plan-view TEM samples, islands were observed, which began to coalesce at a thickness of $\approx$12 nm forming 90° twin domains. By analysis of the Moiré patterns we noted an increasing relaxation of the in-plane lattice parameters of the $Bi_2Sr_2CaCu_2O_x$ phase with increasing film thickness. No $Bi_2Sr_2CaCu_2O_x$ phase was seen in cross-section TEM samples up to a film thickness of 12.5 nm inclusive but two unidentified phases with a fringe spacing in [001] direction of the $SrTiO_3$ of $\approx$3.3 Å and $\approx$8 Å, respectively. The first one occurred often in discrete film thicknesses of 4, 8 and 12 nm, the other one did not. We suggest, that a precursor mechanism for the growth of the ultrathin $Bi_2Sr_2CaCu_2O_x$ films exists. AFM investigations showed a three stage growth mechanism: 1. appearance of small circular nuclei with a tendency to coalesce, 2. islands form a facet-like film surface and 3. smooth surface. An high density of small holes clustering round needlelike outgrowths was seen in 12.5-nm and thicker films.

1. Introduction

Since the discovery of high-T_c superconducting oxides, much attention has been attracted to the epitaxial film growth of these materials, on one hand to get control of the final microstructure of the film by varying the preparation conditions, on the other hand for the study of basic physics. It is well known, that the physical properties of the oxide materials are sensitive to the preparation conditions [*e.g.* 1,2] and the resulting microstructure [*e.g.* 3]. One way for a comprehensive understanding of this behaviour is to study the epitaxial growth mechanism of thin films in early stages, starting from the nucleation and the growth of a few monolayers up to bulk growth.

Two different methods are known for the characterization of the $YBa_2Cu_3O_y$ growth mechanism on MgO or $SrTiO_3$ substrates. Either thin films are explored during their growth, e.g. by the in-situ observation of reflection high-energy electron-diffraction (RHEED) oscillations [4] or ultrathin films are examined, in which deposition is stopped after a definite mean coverage followed by an ex-situ microstructure analysis, e.g. by scanning tunneling (STM) [5,6] or transmission electron microscopy (TEM) [3,7]. Up to now only a few reports are known which investigate the growth of $Bi_2Sr_2Ca_{n-1}Cu_nO_{4+2n+\delta}$ thin films [8,9].

In this paper, we report TEM and atomic force microscope (AFM) investigations of ultrathin $Bi_2Sr_2CaCu_2O_x$ films on (001) $SrTiO_3$ substrates.

2. Experimental procedures

Thin films of $Bi_2Sr_2CaCu_2O_x$ were prepared onto (001) $SrTiO_3$ substrates by pulsed laser deposition. Details of the deposition process and the electrical properties of such c-axis-oriented thin films have been reported elsewhere [2]. Three series, each with six nominal film thicknesses of 3, 6, 12.5, 25, 50 and 100 nm (corresponding to 1, 2, 4, 8, 16, and 32 c-unit cells), were investigated. These values are extrapolated from deposition rates for thicker films. TEM-cross-section samples were prepared from a through-thickness series with an 100 nm thick protective overlayer of amorphous $Bi_2Sr_2CaCu_2O_x$, plan-view samples from a series of films without this overlayer, each by using standard techniques [9]. Electron microscopy was performed using JEOL 2000EX, JEOL 4000EX and 4000FX electron microscopes operated at 200 kV and 400 kV, respectively. The third series has been used to study the surface morphology, determined by AFM using a Nanoscope III with a silicon single crystal tip operating in contact mode.

0925-8388/93/$06.00

3. Results

3.1 Inductively measured transition temperature

The inductively measured transition temperature T_c as a function of the film thickness for several superconducting thin films with a mean thickness of 12.5 to 720 nm is presented in Fig.1. $T_c(50\%)$ shows an increase of T_c and a decrease of the transition width $\Delta T_c = T_c(90\%) - T_c(10\%)$ with increasing film thickness up to 150 nm. No dependence is observed for thicker films, the $T_c(50\%)$ remains constant at 76 K with $\Delta T_c < 3$ K. An inductively measured transition temperature could be observed down to a 12.5-nm thick film with $T_c(50\%) \approx 11$ K (*see inset of Fig. 1*).

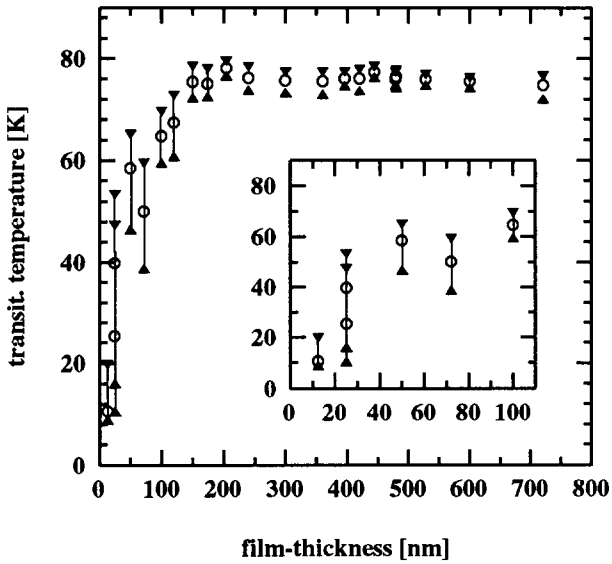

Fig. 1. Film thickness dependence of the inductively measured T_c for $Bi_2Sr_2CaCu_2O_x$ thin films grown on (001) $SrTiO_3$. The area bars indicate the $\Delta T_c = T_c(90\%) - T_c(10\%)$. The open circles represent the midpoint of the transition curve $T_c(50\%)$. The inset shows a stretched part for the ultrathin films.

3.2 Transmission electron microscopy

3.2.1 Plan-view

Figure 2 shows a plan-view micrograph of a 25-nm thick film taken along the $Bi_2Sr_2CaCu_2O_x$ [001] zone axis direction. The inset exhibits the corresponding selected-area electron diffraction pattern. The Moiré fringe contrast in plan-view images arises from the difference of the two overlapping crystal foils of $SrTiO_3$ and $Bi_2Sr_2CaCu_2O_x$. Moiré pattern and the fringe contrast of the b-modulation structure of the $Bi_2Sr_2CaCu_2O_x$ phase were used to detect holes in the film. The validity of this procedure was examined by energy-dispersive x-ray microanalysis (EDX) in a TEM. In Moiré-free regions the EDX investigations of the 25-nm thick film sample showed a strong decrease - by a factor of ten - of the copper, bismuth and calcium signals in comparison to regions with Moiré fringe contrast. This confirms, that the film in "bare" regions is by far thinner than elsewhere. Thus, we assume that at this stage of deposition the film consists of interconnected islands, a few hundreds of nanometers in size and - by analysis of the direction of the b-modulation of the film - forming 90°-twin domains. Regions with high and low island densities were observed. Hence, we suggest that there exists the tendency for nuclei to cluster nonuniformly. The frequent curving of the Moiré fringes indicates that the film is heavily strained.

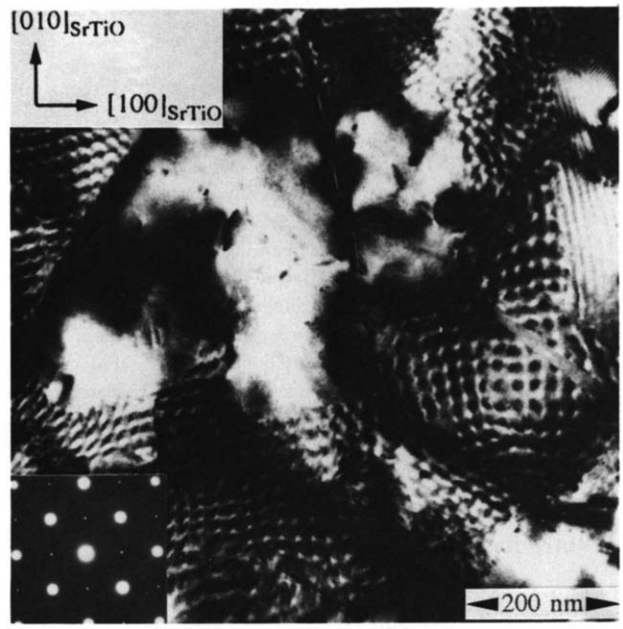

Fig. 2. Plan-view micrograph of a 25-nm thick $Bi_2Sr_2CaCu_2O_x$ film grown on (001) $SrTiO_3$ taken along the [001] direction of the film. The dominant Moiré fringes are oriented along the [110] and [-110] directions of the film. The inset shows the selected-area electron diffraction pattern.

Table 1. Fringe spacings d_{f110} of the $Bi_2Sr_2CaCu_2O_x$ phase in the [110] direction of the film as a function of the deposited film thickness.

dep. film thickness [nm]	d_{f110} [Å] from plan-view	cross-section
100	-in work-	≈3.8 Bi-2212
50	3.848-3.857	-in work-
25	3.863-3.869	<3.9 Bi-2212
12.5	3.867-3.874	≈3.9 A+B
6	no Moiré	>3.9 A+B

Down to the 12.5-nm thick film, we could derive the in-plane lattice parameters of the film from the Moiré pattern with large fringe spacings by an exactness of 0.003 Å neglecting rotational misalignment effects of the Moiré pattern. Thinner films do not show this pattern. The results for the fringe spacing along the [110]

direction of the film d_{fl10} are listed in table 1. The given intervals for each film thickness represent the spread of the measured values by analysis of many kinds of islands in one film. We conclude from the thickness dependence of d_{fl10}, that the relaxation of the in-plane lattice parameters of the $Bi_2Sr_2CaCu_2O_x$ phase proceeds with increasing film thickness. A variable film thickness of the islands can cause the d_{fl10} spread in each film.

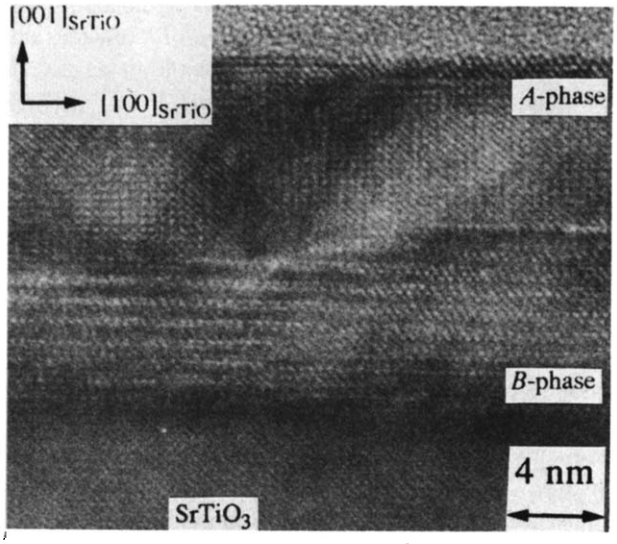

Fig. 3. A cross-section micrograph of a 12.5-nm thick $Bi_2Sr_2CaCu_2O_x$ film grown on (001) $SrTiO_3$.

3.2.2 Cross-section

Figure 3 shows a cross-section micrograph of a 12.5-nm thick film formed on the $SrTiO_3$ [010] zone axis. The two occurring phases are labeled with *A* and *B*. From the corresponding optical diffraction patterns we calculate the lattice parameters with a precision of approximately ± 0.1 Å. Parallel to the [100] direction of $SrTiO_3$ we found a fringe spacing of the *A*-phase of 3.8 to 3.9 Å, parallel to the $[001]_{SrTiO}$ direction ≈ 3.3 Å. For the *B*-phase we get a fringe spacing of ≈ 3.9 Å parallel to the $[100]_{SrTiO}$ axis and ≈ 8 Å parallel to the $[001]_{SrTiO}$ axis. As shown in Fig. 3, we always observe the *B*-phase covered by the *A*-phase in 6- and 12.5-nm thick film samples. Furthermore, the *A*-phase occurs often with discrete film thicknesses of 4, 8 and 12 nm, except at edges of islands. The *B* phase does not show this tendency, the thickness ranges from 3 to 10 nm. However, both phases occur only with an almost equal or smaller film thickness than calculated from the deposition rate. The $Bi_2Sr_2CaCu_2O_x$ phase was not detected in both samples.

Figure 4 is a representative image of a nominally 25-nm thick film. Here, the actual film thickness amounts to 32 nm, but varies from 20 to 32 nm in the whole examined film area. The inset shows the optical diffraction pattern of the film. The lattice parameters along the $[100]_{SrTiO}$- and $[001]_{SrTiO}$-directions can be measured to be 3.8-3.9 Å and 3.1 nm, respectively. By this we identify the film as the orthorhombic $Bi_2Sr_2CaCu_2O_x$ phase with the crystallographic [001] and [110] directions of the film parallel to the [001] and [100] directions of the substrate, in accordance to the work of Zhang et al. [9].

The phases *A* and *B* could never be detected in films equal or thicker than 25 nm, whereas the orthorhombic $Bi_2Sr_2CaCu_2O_x$ phase exists from the interface substrate/film up to the interface film/amorphous overlayer, as shown in Fig.4. The phases, which are present in our TEM cross-section samples, are listed in table 1 together with the scalings of the fringe spacings along the $[100]_{SrTiO}$-direction calculated from the corresponding optical diffraction patterns.

With focussing on the phases *A* and *B*, EDX analysis in conjunction with high-resolution microscopy of the 12.5-nm thick film showed no hint to the absence of one of the elements bismuth, strontium, calcium or copper.

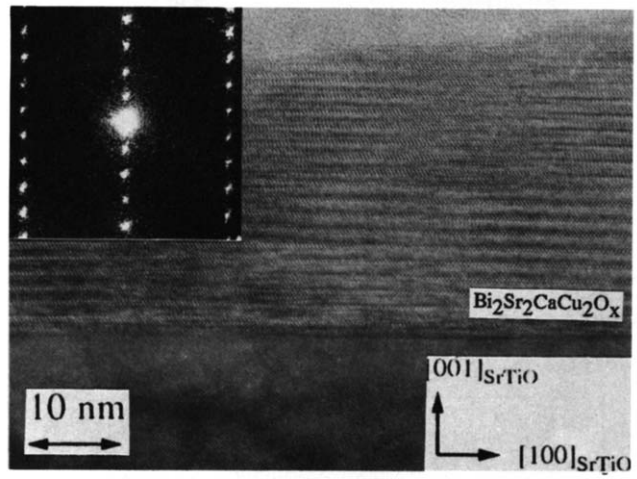

Fig. 4. A cross-section micrograph of a 25-nm thick $Bi_2Sr_2CaCu_2O_x$ film grown on (001) $SrTiO_3$. The inset shows the optical diffraction pattern of the film.

3.3 Atomic force microscopy

Figure 5 shows an AFM image of a nominally 6-nm thick film. The observed area is 0.7 μm by 0.7 μm. An high quantity of circular nuclei can be seen differing from each other in form and size. The lateral extension scales from a few tens of nanometers up to 200 nm. The nuclei indicate a tendency to coalesce forming plateaus. The height of these plateaus is almost homogeneous and amounts to 2-3 nm. The edges do not show a preferential alignment.

Figure 6 shows an AFM image of a nominally 25-nm thick film. The observed square dimension is 1.5 μm by 1.5 μm. A distinct faceting of the film can be seen with an alignment of the edges along the diagonals of the image equal to the [100] and [010] directions of the film. The lateral extension of the facet-like islands in both directions ranges from a few hundreds of nanometers up

to a few micrometers. In between, we observe thinner regions, sometimes gaps with a width of a few tens of nanometers sometimes large areas with lateral extensions up to 100 nm. The surface of the facets is covered by small nuclei, each only a few nanometers in size. The density of the nuclei is estimated to be $5 \cdot 10^{10}$ cm^{-2}. The roughness of the surface is smaller than 6 nm.

In thicker films, like a 50-nm thick film, we observe a rather complete and flat film surface. The mean root square roughness of an area of 1 μm^2 can be derived to be 3.5-4.5 nm by a maximum value of the difference (top to bottom) of 8-9 nm.

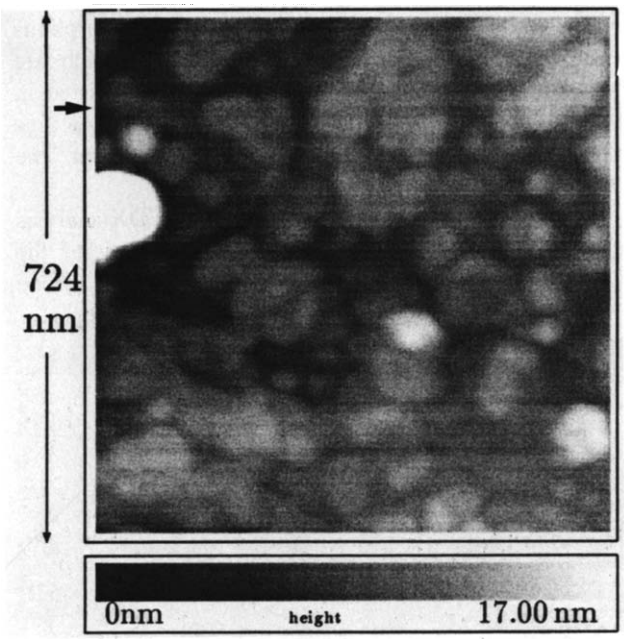

Fig. 5. AFM image of a 6-nm thick $Bi_2Sr_2CaCu_2O_x$ film grown on (001) $SrTiO_3$.

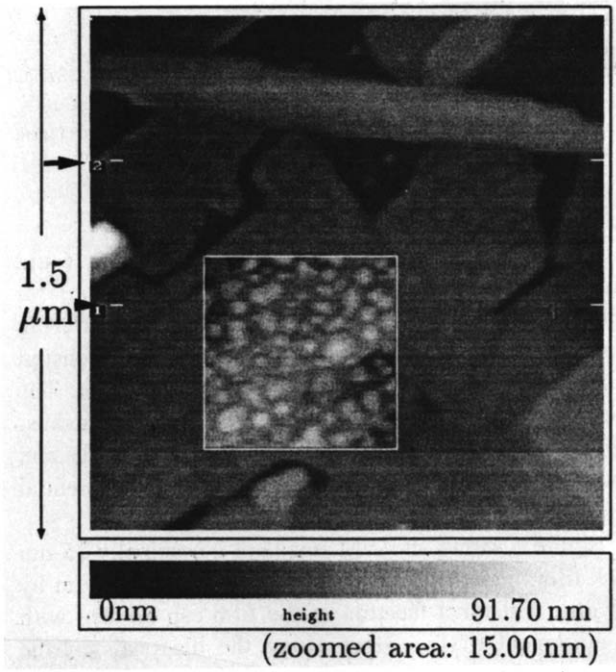

Fig. 6. AFM image of a 25-nm thick $Bi_2Sr_2CaCu_2O_x$ film grown on (001) $SrTiO_3$.

Additionally, we observe needlelike outgrowths, a few micrometers long and a few hundreds of nanometers wide, always aligned along two orthogonal directions parallel to the [100] and [010] directions of the substrate. The density could be estimated to $2 \cdot 10^7$ cm^{-2}. Close to each outgrowth we can find a clustering of holes in the film with a lateral extension of a few tens up to a few hundreds of nanometers. We could never detect growth spirals in all examined films.

4. Conclusions

The absence or less occurrence of the $Bi_2Sr_2CaCu_2O_x$ phase in 6- and 12.5-nm thick film cross-section samples in conjunction with the appearance of two still unidentified phases let us suppose the following process for the growth of $Bi_2Sr_2CaCu_2O_x$ on $SrTiO_3$: the *A*- and *B*-phases may be two successive precursors of the $Bi_2Sr_2CaCu_2O_x$ phase. A phase-transition occurs at a typical thickness $t > 12$ nm. Then the absence of the $Bi_2Sr_2CaCu_2O_x$ phase in the 12.5-nm thick film cross-section sample may be due to the examination of islands with a thickness less than the typical thickness.

From the AFM investigations we conclude that a three stage growth mechanism takes place: 1.) 3- and 6-nm thick films have a high density of circular nuclei which begin to coalesce forming plateaus with homogeneous height. 2.) These plateaus coalesce to facet-like islands in 12.5- and 25-nm thick films. The islands were separated by small gaps (≈ 10 nm wide). 3.) Thicker films show a smooth and complete surface only disturbed by needlelike outgrowths.

We would like to thank P. Bauer for his assistance in AFM measurements and P. Schmitt for stimulating discussions. The AFM investigations were supported by the Bayerische Forschungsstiftung Hochtemperatursupraleitung (FORSUPRA).

References

[1] B. Roas et al., Appl. Phys. Lett. **53**, 1557 (1988)
[2] P. Schmitt et al., Physica C **168**, 475 (1990)
[3] S. K. Streiffer et al., Phys. Rev. B **43**, 13007 (1991)
[4] T. Terashima et al., Phys. Rev. Let. **65**, 2684 (1990)
[5] D. P. Norton et al., Phys. Rev. B **44**, 9760 (1991)
[6] X. Y. Zheng et al., Phys. Rev. B **45**, 7584 (1992)
[7] T. Satoh et al., Physica C **185-189**, 2033 (1991)
[8] T. Sugimoto et al., Physica C **185-189**, 2045 (1991)
[9] X. F. Zhang et al., Physica C **183**, 379 (1991)